Nucleation mechanisms of epitaxial GaN nanowires: Origin of their self-induced formation and initial radius

V. Consonni, M. Knelangen, L. Geelhaar, A. Trampert, and H. Riechert

Paul-Drude-Institute for Solid State Electronics, Hausvogteiplatz 5-7, 10117 Berlin, Germany

The formation mechanisms of epitaxial GaN nanowires grown within a self-induced approach by molecular-beam epitaxy have been investigated at the onset of the nucleation process by combining *in situ* reflection high-energy electron-diffraction measurements and *ex situ* high-resolution transmission electron microscopy imaging. It is shown that the self-induced growth of GaN nanowires on the AlN buffer layer is initially governed by the nucleation of dislocation-free coherent islands. These coherent islands develop through a series of shape transitions from spherical caps through truncated to full pyramids in order to elastically relieve the lattice-mismatch-induced strain. A strong correlation between the subsequent process of plastic relaxation and the final shape transition from full pyramids toward the very first nanowires is found. The experimental critical radius at which the misfit dislocation nucleates is in very good agreement with the theoretical critical radius for the formation of the misfit dislocation in full pyramids, showing that the plastic relaxation process does take place within full pyramids: this critical size corresponds to the initial radius of the very first nanowires. We associate the plastic relaxation of the lattice-mismatch-induced strain occurring within full pyramids with a drastic change in their total free energy: this gives rise to a driving force for the shape transition toward the very first nanowires, which is mainly due to the anisotropy of surface energy.

I. INTRODUCTION

Semiconductor nanowires (NWs) have received in the last decade increasing basic and technological interest. On the one hand, their high aspect ratio in the nanoscale dimensions gives rise to novel physical processes and remarkable properties.[1] On the other hand, their suitable compatibility with silicon-based technology without the use of advanced lithography is very promising since it opens the way to a wide variety of potential nanodevice applications.[2–5] Up to now, the most famous way to induce the formation of NWs is the well-known vapor-liquid-solid mechanism, for which a catalyst, typically gold droplets, is used.[6] Several growth models have been developed to account for the catalyst-induced approach: most of them consider gold droplets as collectors for the different species and NW growth becoming prevalent when supersaturation in these droplets is reached.[7,8] The catalyst-induced growth thus supplies highly dense ensembles of well-separated NWs with a homogeneous radius strongly governed by the gold droplet size. Nevertheless, recent papers have pointed out that the NW contamination by the catalyst considerably limits their structural and optical quality.[9–11]

Increasing efforts have therefore been dedicated to the understanding and control of catalyst-free NW growth through the oxide-assisted, template-assisted, selective-area or self-induced approach, for example.[12] The latter has the advantage that it does not involve any foreign material at all. This approach commonly employs specific growth conditions, which are often opposite to the growth conditions of two-dimensional (2D) layers of the same material: a highly nitrogen-rich vapor phase is required for the self-induced growth of GaN NWs by plasma-assisted molecular-beam epitaxy (PAMBE) and often combined with a high growth temperature.[13–16] However, very few basic works have been

devoted to investigate the physical mechanisms that can account for the self-induced growth and especially for the specific nucleation processes.[17–21] In the following, we focus on the GaN/AlN material system: although the majority of the physical aspects depends on the material system considered, some findings discussed here can be applied to other closely related material systems, in particular, belonging to the III/V and II/VI semiconductor groups.

It was early proposed that the formation of gallium droplets could be responsible for GaN NW growth by PAMBE, similarly to the catalyst-induced growth, but the presence of these assumed droplets has never been confirmed.[22,23] It was also mentioned that different diffusion lengths or different sticking coefficients on the involved GaN facets could account for the self-induced NW growth: a larger diffusion length or a smaller sticking coefficient were proposed for gallium adatoms on the $\{1\bar{1}00\}$ planes of vertical sidewalls as compared to gallium adatoms on the $\{0001\}$ plane of the top facet.[24,25] Lymperakis *et al.*[26] recently showed by first-principles calculations a strong in-plane anisotropy of the diffusion barriers on nonpolar GaN surfaces for gallium adatoms, revealing that the single diffusion-induced mechanism operates but is not enough to completely account for the self-induced NW growth. Therefore, Foxon *et al.*[27] also suggested that geometric effects in the MBE chamber could play a non-negligible role. Nevertheless, the last mechanisms are based on the prerequisite that the very first NWs have already nucleated and cannot account for their formation. For the self-induced approach, a clear distinction is necessary between the nucleation phase, which defines the position and, presumably, the radius of NWs, and the subsequent growth phase, resulting in a lengthening of the NW nuclei. Songmuang *et al.*[17] mentioned that GaN three-dimensional (3D) islands are formed according to an assumed initial Stranski-Krastanov mechanism and could act as a seed for

the subsequent growth of GaN NWs at their top. Calarco *et al.*[18] also stressed the fact that the nucleation process is kinetically slow and could be defined as the process during which the GaN NW density increases before reaching a maximum. The aim of this paper is to cast a new light concerning the nucleation mechanisms occurring during the self-induced growth of epitaxial GaN NWs, which give rise to the very first NWs, and especially to focus on their relationship with the plastic relaxation process.

In this paper, we study the nucleation process of GaN NWs by combining *in situ* reflection high-energy electron-diffraction (RHEED) measurements and *ex situ* high-resolution transmission electron microscopy (HRTEM) imaging. It is shown that the self-induced growth of GaN NWs on the AlN buffer layer occurs through the initial formation of dislocation-free coherent spherical-cap-shaped islands at the onset of the nucleation process: subsequently, these islands exhibit successive shape transitions, which aim at relieving the lattice-mismatch induced strain and at minimizing their total free energy per unit volume. A strong correlation between the plastic relaxation process occurring within full-pyramid-shaped islands and the subsequent shape transition toward the very first NWs is found. The experimental critical radius, which is required to nucleate the misfit dislocations within such nanostructures, is compared to the predicted radii obtained from theoretical approaches given by Tillmann and Förster[28] and Glas,[29] which describe the misfit dislocation formation in pyramid-shaped islands and NWs, respectively. Interestingly, such a critical size can directly be related to the initial radius of the very first NWs. Furthermore, simple thermodynamic considerations are taken into account to illustrate the pronounced change in the total free energy of full-pyramid-shaped islands induced by their complete relaxation and to highlight the driving force for the shape transition toward the very first NWs.

II. EXPERIMENT

A. Self-induced NW growth conditions

All samples were grown on Si(111) substrates by radio-frequency PAMBE. The active atomic nitrogen and gallium atoms were supplied by a plasma source operating at 500 W power with 2 sccm flux and by a thermal effusion cell, respectively. Prior to the GaN NW growth, a 5-nm-thick AlN buffer layer was deposited on the Si(111) substrate in order to ensure an epitaxial relation with the GaN NWs: the aluminum atoms were accumulated on the substrate surface at 800 °C and then exposed to the active atomic nitrogen flux for 5 min to induce a nitridation process. The resulting AlN buffer layer is completely relaxed, as revealed by x-ray diffraction measurements. GaN NWs were eventually grown at a high substrate temperature of 800 °C under highly nitrogen-rich conditions. The nominal gallium (nitrogen) flux corresponding to the growth rate of GaN planar layer deposited on a SiC(111) substrate under nitrogen-rich (gallium-rich) conditions was first determined so as to assess the V/III ratio, which equals 10. All samples were continuously rotated in order to ensure the flux and temperature homogeneity on the surface.
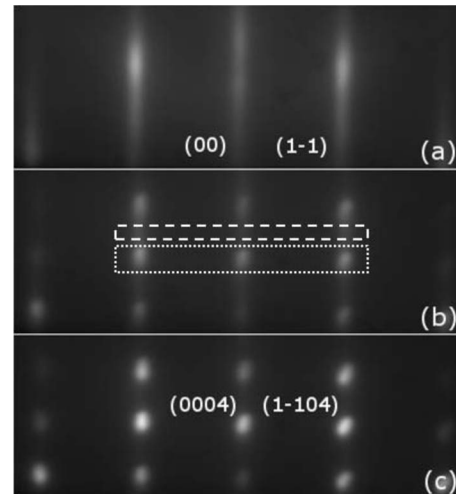

FIG. 1. Typical RHEED patterns of (a) the AlN buffer layer (2 min), (b) the GaN pyramid-shaped island at the onset of the nucleation process (10 min), and (c) the GaN NWs (17 min). The rectangular areas depicted by dashed and dotted white lines are used. The former area yields the AlN streak intensity, whereas the latter area yields its sum with the GaN spot intensity as growth proceeds.

B. Structural analysis

In situ RHEED measurements were performed during the entire growth process along the $[11\bar{2}0]$ azimuth using an electron gun operating with a 2 A filament current and 20 kV acceleration voltage. The incident-beam angle with the sample was 3°. A programmable motor was used to stop the rotation with high reproducibility at a precisely defined position in order to record one RHEED pattern every 20 seconds. Three typical RHEED patterns collected on the sample at different growth durations are represented in Fig. 1. The presence of a smooth AlN buffer layer on the Si(111) substrate leads to a streaky (1×1) 2D reflection pattern, as shown in Fig. 1(a). In contrast, the nucleation of GaN islands is characterized by a spotty 3D transmission pattern. The lateral positions of the GaN spots and AlN streaks are very close as seen in Fig. 1(b) since the lattice mismatch between AlN and GaN is 2.41%.[30] As growth proceeds, the RHEED images undergo a transition from streaky 2D reflection to spotty 3D transmission patterns, as represented in Fig. 1.

In the following, the RHEED intensity of the AlN streaks and of its sum with the GaN spots was determined by monitoring *in situ* the different contributions coming from diffraction. Accordingly, two sets of analysis regions with given positions and fixed surface areas were selected in each RHEED pattern, as depicted by the dashed and dotted white rectangles in Fig. 1(b). The evolution of the AlN streak intensity and of its sum with the GaN spot intensity was then assessed as follows: a Gaussian fit procedure was first carried out and the intensity of the AlN streaks and of its sum with the GaN spots was second determined by summing the overall area under each Gaussian fit. We define in the following the overall intensity as the sum of the AlN streak intensity with the GaN spot intensity. We point out that the GaN spot intensity cannot be measured separately from the AlN streak intensity within such an analysis procedure.

In order to combine these RHEED measurements with a microstructural analysis, cross-sectional TEM specimens from dedicated samples grown at different durations of 4.5, 6, 9, 10, 12, and 15 min were prepared by mechanical lapping and polishing, followed by argon-ion milling according to standard techniques. HRTEM imaging and selected-area electron-diffraction (SAED) patterns were achieved with a JEOL 3010 microscope operating at 300 kV so as to image the morphology and orientation of GaN islands and NWs as growth proceeds.

III. RESULTS

A. Nucleation process at the very early stages of self-induced NW growth

The evolution of the two distinct RHEED intensities are presented in Fig. 2. The insets represent simple sketches of the GaN island morphology, as obtained by HRTEM images taken on dedicated samples grown at different durations in Fig. 3. From the evolution of the two distinct RHEED intensities, the nucleation process can be divided into six distinct stages:

1. Stage (I)

As growth starts (i.e., the gallium shutter is opened), the AlN streak intensity continuously decreases for 3.5 min, as shown in Fig. 2(a). In this stage, no 3D transmission spot belonging to GaN is observed on the RHEED patterns, accounting for the identical decrease in the overall intensity in Fig. 2(b). Gallium atoms adsorb onto the AlN buffer layer, freely diffuse, desorb, or aggregate with other atoms to form GaN 2D metastable nuclei.[31] As these surface processes result in a progressive surface coverage of the AlN buffer layer, the decrease in the AlN streak intensity is continuous and induced by diffuse scattering processes. The AlN streak intensity in stage (I) is thus considered as a direct measurement of the AlN surface coverage by gallium adatoms and 2D GaN nuclei. The continuous decrease is also consistent with the absence of the formation of a complete continuous 2D wetting layer, as discussed below.

2. Stage (II)

The start of stage (II) after a growth time of about 3.5 min is marked by an increase in the overall intensity in Fig. 2(b). This growth time corresponds to the occurrence of the first 3D transmission spots belonging to GaN on the RHEED patterns: this delay can be defined as an incubation time, which is required to form first GaN 3D stable nuclei.[31] The incubation time is expected to strongly depend on the growth temperature since the formation of critical 3D nuclei is mainly governed by the interplay between the processes of adsorption, desorption, and surface diffusion of gallium and nitrogen adatoms. Indeed, we point out that the growth is achieved at a high substrate temperature of 800 °C, which induces a significant gallium desorption process. Interestingly, the AlN streak intensity still decreases continuously and drastically but with a less pronounced slope from this incubation time until a growth time of 8 min. A typical HR-
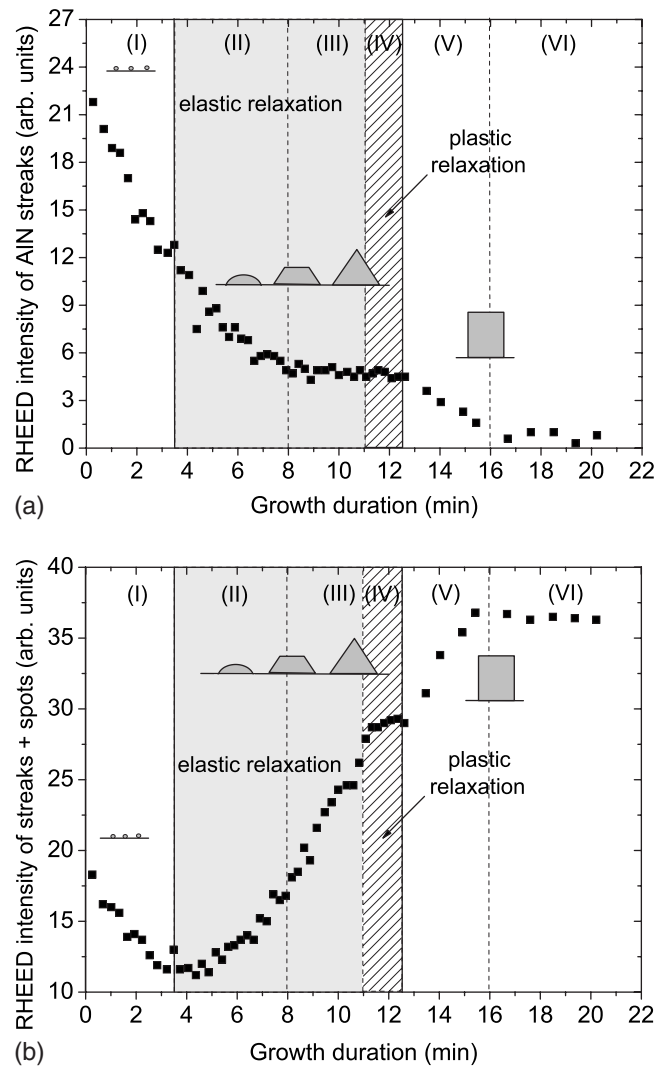

(a)

(b)

FIG. 2. Evolution of the RHEED intensity (a) of AlN streaks and (b) of its sum with the GaN spot intensity as growth proceeds, according to the rectangular areas depicted in Fig. 1. The insets represent simple sketches of GaN island shape, as observed by HRTEM images in Fig. 3 collected on dedicated samples. Six distinct stages are distinguished within such an analysis. The two consecutive regions involving elastic and plastic relaxation processes are deduced from Fig. 4.

TEM image of a GaN 3D nucleus is shown in Fig. 3(a): spherical-cap-shaped islands with a radius of 2 nm and a height of 1 nm are formed on the surface upon the onset of the nucleation process. As growth proceeds, the density of spherical caps continuously increases: these islands cover more and more surface of the AlN buffer layer, which can account for the abrupt decrease in the AlN streak intensity. Island coarsening could also contribute to the decrease in the AlN streak intensity, as growing islands also cover more and more surface, but this effect is expected to be much less pronounced. Interestingly, no sign for the presence of a complete continuous 2D wetting layer is observed by HRTEM images neither during the stage (I) nor during the stage (II) [see the inset of Fig. 3(a)]. The absence of a wetting layer, for which the presence is widely mentioned for the growth of
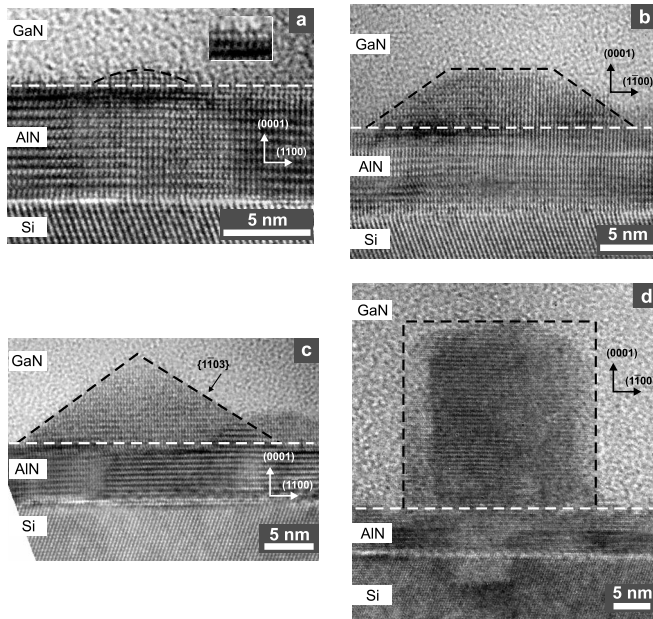
FIG. 3. HRTEM images collected on dedicated samples grown during 4.5, 6, 9, 10, and 15 min, revealing the following respective GaN island shapes at the onset of the nucleation process: (a) spherical-cap-shaped island with an inset representing a high magnification of the first AlN monolayers at the interface, (b) truncated-pyramid-shaped island, (c) full-pyramid-shaped island, and (d) NW. The pyramid-shaped island and NW are hexahedral: the full-pyramid-shaped island presents a facet angle of 32° with respect to the {0001} plane, suggesting that the {1$\bar{1}$03} side facet is involved. All the island shapes are outlined for the sake of clarity.

GaN quantum dots (QDs) on the AlN buffer layer,[32,33] could arise from the different conditions used for the growth of GaN NWs. We also point out that the presence of a wetting layer has already been evidenced for the self-induced growth of GaN NWs but on different substrates.[20] Furthermore, an example among all the collected HRTEM images is shown in Fig. 3(b) and reveals the presence of truncated pyramid-shaped islands. GaN islands thus undergo a shape transition from spherical caps to truncated pyramids during this stage. The formation of {0001} top facets (i.e., *c* plane) and of the lateral facets aims at elastically relieving the lattice-mismatch-induced strain: the total free energy per unit volume of each island is reduced by decreasing the stored elastic strain energy more than increasing the surface energy through the newly formed surfaces.[34,35] The nature of the lateral facets in truncated pyramids also changes. A very minority of small truncated pyramids presents a lateral facet angle smaller than 25° with respect to the {0001} plane, suggesting that the {1$\bar{1}$0L} side facets are involved. In contrast, most of truncated pyramids have larger dimensions and present a lateral facet angle of about 32° with respect to the {0001} plane, indicating that the {1$\bar{1}$03} side facets are formed. The presence of these facets has already been mentioned for the growth of GaN QDs on the AlN buffer layer during a Stranski-Krastanov mechanism and has been attributed to their possibly small surface energy.[36,37] These experimental observations suggest that GaN islands undergo a new

shape transition during this stage from truncated pyramids with {1$\bar{1}$0L} lateral facets to truncated pyramids with {1$\bar{1}$03} side facets. It is remarkable that the two shape transitions during this stage results in steeper side facets, thus approaching the NW morphology.

3. Stage (III)

The start of stage (III) after a growth time of 8 min is characterized by an abrupt change in the evolution of the AlN streak intensity: the intensity stops decreasing so as to reach a plateau around this growth time. The saturation of the AlN streak intensity reveals that the island density also saturates and remains constant for a longer growth duration. The growth time necessary to reach this plateau thus corresponds to a similar nucleation time as defined by Calarco *et al.*,[18] but in the case of islands instead of NWs. In contrast, the overall intensity keeps on increasing, as shown in Fig. 2(b). Furthermore, an example among all the collected HRTEM images is shown in Fig. 3(c) and reveals the presence of full pyramid-shaped islands with larger dimensions compared to the sizes of truncated pyramids. GaN islands thus undergo a new shape transition from truncated to full pyramids during this stage. This shape transition suggests that the {0001} top facet shrinks as growth proceeds and is replaced by the {1$\bar{1}$03} lateral facets. Several theoretical approaches account for the preferential pyramidlike shape in the QD growth and in particular for the shape transition from truncated to full pyramids. Such approaches are again based on the minimization of the total free energy per unit volume to predict the preferred island shape, as discussed above.[38,39] Interestingly, the spherical caps, truncated and full pyramids shown in Fig. 3 are coherent, namely, dislocation free. The shape evolution during the stages (I), (II), and (III) thus governs the elastic relaxation process. It is expected that each consecutive predominant island shape is associated with a certain level of increasing strain relaxation.[40]

4. Stage (IV)

Subsequently, the stage (IV) starts with the plastic relaxation process occurring between growth times of 11.5 and 12.5 min. The dislocation nucleation becomes predominant and induces an abrupt strain relaxation toward a completely relieved state. Interestingly, the plastic relaxation occurs at the end of the plateau for the AlN streak intensity, as depicted by the hatched region in Fig. 2(a). The overall intensity also lightly saturates upon the plastic relaxation process as shown in Fig. 2(b), revealing that such a process directly affects the growth mechanisms. An example among all the collected HRTEM images is shown in Fig. 3(d) and reveals the presence of NW-shaped islands: the existence of the {0001} top facet is evidenced together with vertical sidewalls, which are consistent with the presence of {1$\bar{1}$00} planes (i.e., *m* planes) as typically reported in the literature.[19] GaN islands thus undergo a new shape transition from full pyramids to NWs, which is concomitant with the plastic relaxation process, as discussed in details in the following.

5. Stage (V)

The start of stage (V) is revealed by the rapid decrease in the AlN streak intensity after a growth time of 12.5 min, especially once the plastic relaxation process has been completed. Its sum with the GaN spot intensity, namely, mainly the single GaN spot intensity here, increases again at the same time. We point out that the total growth rate of dislocated islands is higher than the growth rate of dislocation-free coherent islands, as theoretically predicted and experimentally observed for the growth of germanium islands on vicinal Si(100) substrates.[41,42] Such an increase in the GaN spot intensity could thus be more related to a significant difference in the growth kinetics induced by the plastic relaxation process rather than to a variation in the NW density. Consequently, the NW height rapidly increases due to the preferential axial growth along the $[0001]$ direction compared to the radial growth along the $[1\bar{1}00]$ direction, which is expected to result in more intense 3D transmission spots belonging to GaN. Simultaneously, shadowing processes prevent the surface of the AlN buffer layer from being probed by the electron beam, resulting in the vanishing of the AlN streak intensity.

6. Stage (VI)

The stage (VI) is defined by the constancy of the main final features of the RHEED patterns after a growth time of 16 min, as NW growth proceeds. The electron beam probes only the NW top region, whose crystallographic structure does not change, without reaching the AlN buffer layer. This feature leads to the vanishing of the AlN streak intensity and the constancy of the GaN spot intensity. The eventual nucleation of new small islands would not be detected by RHEED measurements in stage (VI), which could account for the longer nucleation time obtained by Calarco *et al.*,[18] from *ex situ* electron microscopy measurements of the NW density for different growth durations.

In this section, we have shown that the nucleation mechanisms involved in the self-induced growth of epitaxial GaN NWs retains some similarities with the processes at work in the growth of GaN QDs, although such a series of successive shapes has not been shown explicitly: however, our experimental evidence indicate that GaN nucleates coherently strained on the AlN buffer layer as spherical caps, before a complete continuous 2D wetting layer has been formed. In fact, no sign for the presence of a GaN wetting layer is observed from HRTEM images. Eventually, the nucleation of self-induced GaN NWs strongly differs from the growth of GaN QDs in the subsequent plastic relaxation process: instead of island coarsening and further coalescence as observed for the QD growth, the plastic relaxation process results in the formation of the very first GaN NWs and can therefore be considered as the crucial step in the self-induced approach. We focus in the following on the final shape transition from full pyramids toward the very first NWs and especially on its strong relationship with the plastic relaxation process.
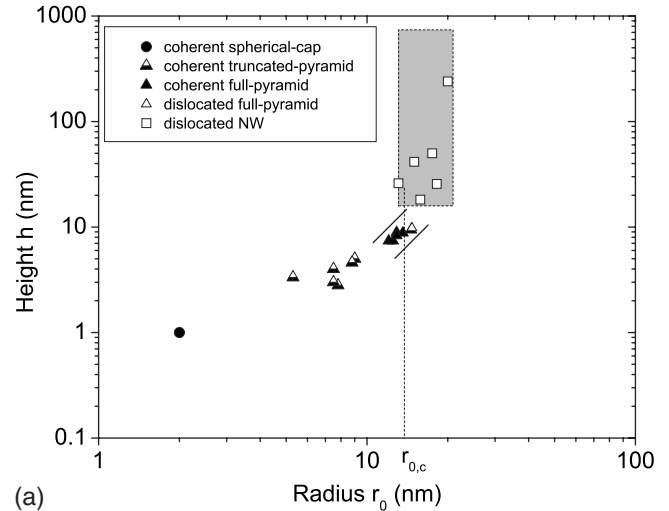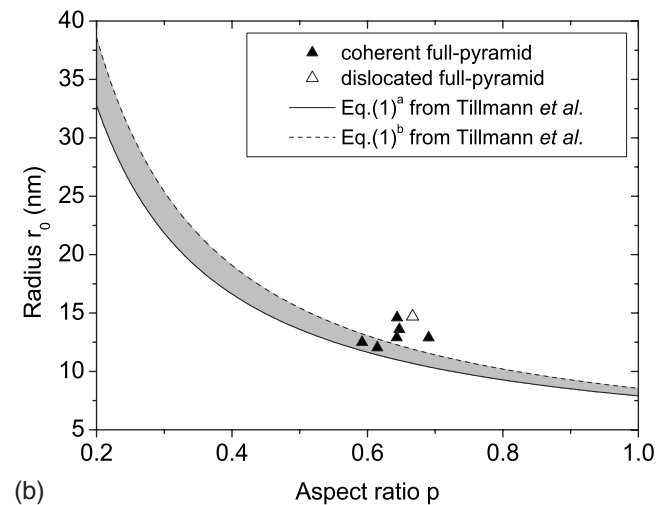
FIG. 4. (a) Height h as a function of radius r_0 obtained from HRTEM images for the different GaN island shapes. The dashed line corresponds to the experimental critical radius $r_{0,c}$ determined for the occurrence of plastic relaxation. (b) Radius r_0 as a function of aspect ratio $p = h/r_0$ obtained from HRTEM images of full-pyramid-shaped islands. The gray color region corresponds to the critical radius $r_{0,c}$ predicted by the approach given by Tillmann and Förster from Eq. (1) with $\varepsilon_0 = 2.41\%$, $b = a = 3.189$ Å, and $\theta = 90°$ for one pure-edge dislocation, $\mu_{AlN} = 142.2$ GPa (solid line: $\nu = 0.203$ and $\mu_{GaN} = 127.8$ GPa from Ref. 45; dashed line: $\nu = 0.353$ and $\mu_{GaN} = 64.9$ GPa from Ref. 46).

B. The role of plastic relaxation process in the final shape transition toward the NW morphology

1. Direct evidence of the relationship between the final shape transition and plastic relaxation

The specific features of islands were systematically determined from HRTEM images recorded on dedicated samples grown at different durations: their shape, their height h, and radius r_0, as well as their relaxation mode (elastic or plastic) were carefully investigated. The experimental data are shown in Fig. 4(a).

First of all, we point out that the experimental observation of islands with various sizes on the same sample can result in

the overlap of two consecutive distinct shapes for a similar growth duration, as represented in the stages (II) and (III) in Fig. 2. This feature is consistent with a long nucleation phase during which new islands form, as previously discussed. Nevertheless, it is clearly revealed in Fig. 4(a) that each island shape corresponds to a specific range of sizes. In other words, each island shape has unique typical dimensions, which are peculiar to it. The successive evolution of the island shape from spherical caps through truncated and full pyramids eventually to NWs with increasing their sizes, namely, with rising the growth duration, as discussed in the last section is thus confirmed in Fig. 4(a).

Second, two distinct regions driven either by elastic or plastic relaxation are distinguished. The elastic-relaxation-driven region, namely, the coherency region, is only composed of spherical caps, truncated and full pyramids, as indicated by the filled icons in Fig. 4(a). The evolution of the island shape in this region aims at minimizing their total free energy per unit volume by elastically relieving the lattice-mismatched-induced strain and accordingly by reducing their stored elastic strain energy, as previously discussed. In contrast, the plastic-relaxation-driven region only involves one full pyramid and all NWs, as revealed by the nonfilled icons in Fig. 4(a). As a consequence, the growth mechanism for the formation of the very first NWs is strongly related to the plastic relaxation process: a critical radius of about 13–14 nm is experimentally deduced in Fig. 4(a), at which the plastic relaxation process occurs and the very first NWs are formed. This experimental radius obviously differs from the critical radius of 3.5 nm, as obtained for the self-induced growth of GaN NWs on the Si(111) substrate.[20] Furthermore, since all full pyramids have identical {1$\bar{1}$03} side facets characterized by an angle of 32° with respect to the {0001} plane, their height h and radius r_0 are correlated: a constant aspect ratio $p=h/r_0$ corresponding to $\tan(32°)=0.62$ is determined. Only a small domain of the elastic-relaxation-driven region is therefore explored by the size range of full pyramids, as indicated by the two delineating straight lines in Fig. 4(a). Interestingly, since the axial growth rate of NWs is much higher than their radial growth rate, NWs longitudinally grow faster. This feature also yields a small-explored domain of the plastic-relaxation-driven region, as represented by the gray color region in Fig. 4(a). In other words, the initial radius of self-induced epitaxial GaN NWs is explicitly defined here by such a gray color region and appears to be strongly governed by the plastic relaxation process.

2. Occurrence of plastic relaxation within full-pyramid-shaped islands

In order to investigate whether the dislocation nucleation occurs before or after the final shape transition toward the NW morphology, theoretical aspects are presented here concerning the occurrence of plastic relaxation in heterostructures. Two theoretical works based on the physical model given by Matthews and Blakeslee[43] are considered to elucidate whether the dislocation nucleation occurs within full pyramids or within NWs.

The model of Matthews and Blakeslee[43] is designed for the case of epitaxial planar layers and considers the energy

balance in equilibrium between the stored elastic strain energy, which increases with film thickness, and the energy cost to nucleate one misfit dislocation. Beyond a critical film thickness, it is predicted that the elastic strain energy reaches a threshold, from which the formation of one misfit dislocation is energetically favorable: the predicted critical thickness is in relatively good agreement with experimental results for many material systems although kinetic limitations are also expected to play a direct role.

Several theoretical approaches describe the critical sizes required to induce plastic relaxation in epitaxial heterostructures instead of elastic relaxation from their lateral surfaces.[28,29,44] Recently, Tillmann and Förster[28] adapted the approach given by Matthews and Blakeslee to the case of epitaxial 3D islands with a wide variety of distinct geometries. By balancing the strain energy gain related to the plastic relaxation process and the energy associated with the strain field of the misfit dislocation, the critical radius $r_{0,c}$ for full pyramids with the height h and the radius r_0 is given as a function of the aspect ratio $p=h/r_0$ by the implicitly defined relation,[28]

$$
r_{0,c} = \frac{2}{b_{eff} \cdot \varepsilon_0} \times \left\{ \frac{b_{eff}^2}{8(1+\nu_{GaN})} + \left[\cos^2\theta + \frac{\sin^2\theta}{1-\nu_{GaN}} \right] \right.
$$
$$
\times \left[\ln\left(\frac{r_{0,c}\sqrt{p}\left(1 - \sqrt{1-\frac{\pi^2}{16}}\right)}{|\vec{b}|} \right) + 1 \right]
$$
$$
\left. \times \left[\Gamma(\lambda,V)\frac{1-\nu_{GaN}}{1+\nu_{GaN}}\frac{\mu_{AlN}|\vec{b}|^2}{\mu_{AlN}+\mu_{GaN}} \right] \right\} \tag{1}
$$

in which μ_{GaN} and μ_{AlN} are the respective shear moduli of GaN and AlN, ν_{GaN} is the Poisson's ratio of GaN, ε_0 is the lattice mismatch between GaN and AlN, **b** is the Burgers vector of the misfit dislocation and b_{eff} its edge component, θ is the angle between the dislocation line and the Burgers vector. $\Gamma(\lambda,V)$ represents a geometric factor depending on the length of the misfit dislocation λ and of the island volume V: $\Gamma(\lambda,V)=\lambda r^2/(4\pi V)=3/(8\pi p)$ for full pyramids. The experimental data of the typical size for full pyramids are gathered in Fig. 4(b) and superimposed to the border region delimiting the elastic- and plastic-relaxation-driven regions, as predicted by Tillmann and Förster in Eq. (1). The border region between the dashed and solid lines is broad and takes into account the uncertainty of the mechanical constants used for GaN.[45,46] It is clearly shown that the approach given by Tillmann and Förster is in very good agreement with the experimental data: the critical radius $r_{0,c}$ to nucleate one misfit dislocation in GaN islands deposited on the AlN buffer layer is found to be around 13–14 nm from experimental results and around 11.5–13 nm from Eq. (1) for the full pyramid morphology.

More recently, Glas[29] adapted the approach given by Matthews and Blakeslee to the case of epitaxial cylindrical-shaped NWs. Very good agreement with experimental results

in the InAs, InP, GaAs/Si material systems have been reported.[47] By determining the excess energy of one dislocated NW with respect to the similar dislocation-free NW, a critical radius $r_{0,c}$ is obtained by the following relation:[29]

$$\frac{2\pi}{A_\nu}\left(\frac{4b_{eff}^2}{\pi^2} - \frac{4b_{eff}\varepsilon_0 r_{0,c}}{\pi}\right) + \frac{(1-\nu_{GaN}\cos^2\theta)b^2}{2\pi(1+\nu_{GaN})}\left(1+\ln\frac{2r_{0,c}}{\pi b}\right)$$
$$= 0 \qquad (2)$$

in which A_ν is a numerical constant weakly dependent upon the Poisson's ratio, which equals 27.3 ± 0.55 for $\nu=1/3$. In contrast to the approach given by Tillmann and Förster, the Glas approach is not in agreement with the experimental data, since a critical radius $r_{0,c}$ of about 32–36 nm to nucleate one misfit dislocation is deduced from Eq. (2) for the NW morphology. We note further that such a critical radius is larger for the NW morphology than for the full pyramid geometry, showing the high efficiency of NWs to elastically relieve the lattice-mismatch-induced strain from their lateral surfaces.

As a consequence, one can deduce that the agreement of experimental data with the approach given by Tillmann and Förster, and not with the Glas approach provides the strong evidence that the plastic relaxation process, namely, the nucleation of the misfit dislocation, occurs within full pyramids and not within NWs. In other words, the plastic relaxation process takes place before the island shape changes toward the NW morphology. The shape transition does occur from dislocated full pyramids to dislocated NWs as growth proceeds. It is further remarkable that the initial radius of the very first NWs directly corresponds to the critical radius required to nucleate the misfit dislocation within full pyramids.

3. Specific mechanisms of plastic relaxation

On the one hand, a full pyramid with one misfit dislocation is represented in Fig. 5. The dislocation is located very close to the island edges, as revealed by the inset of Fig. 5. Such a spatial position suggests that the misfit dislocation nucleates at the island edges where the strain concentration is maximal, as theoretically predicted and experimentally observed in the $In_xGa_{1-x}As/GaAs$ material system, for instance.[44,48,49] The misfit dislocation is of mixed type with a Burgers vector of $(1/3)\langle 11\bar{2}0\rangle$ and retains a dominant edge component.

On the other hand, the misfit dislocation within the NW is located close to its center but not completely in its center, as revealed in Fig. 6. Marzegalli *et al.*[50] evidenced that the relative energy gain in domed- and barn-shaped island in the SiGe/silicon material system is at its maximum when the dislocation is located close to the center at a distance of 0.3 times its diameter. The misfit dislocation within the NW may thus be located where its efficiency is maximal for the overall strain relaxation. Indeed, the SAED pattern of the dislocated NW in the inset of Fig. 6 reveals that the NW is completely relaxed: from a line scan along the $\langle 1\bar{1}00\rangle$ direction, an in-plane lattice parameter of 3.19 ± 0.01 Å is found, indicating that one misfit dislocation is sufficient to entirely relieve the lattice-mismatch-induced strain.
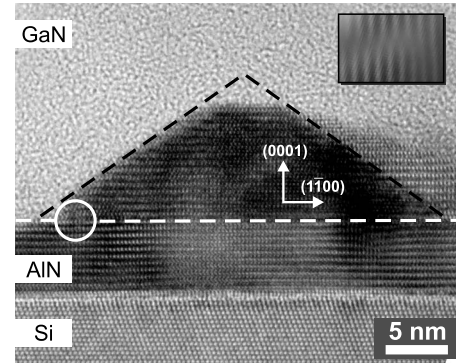

FIG. 5. HRTEM image of a dislocated full-pyramid-shaped island collected on a sample grown during 12 min. The misfit dislocation is located within the white circle, which is close to the island edges. The inset reveals a Fourier-filtered enhancement showing only the $\{1\bar{1}00\}$ lattice planes. The dislocation is mixed with a Burgers vector of $(1/3)\langle 11\bar{2}0\rangle$ and retains a dominant edge component. Note that the full-pyramid-shaped island exhibits one top facet due to its cut during the TEM sample preparation.

As the radii of dislocated full pyramids and dislocated NWs are similar, one can infer that the motion of the misfit dislocation within full pyramids accounts for its spatial position change observed inside the two distinct morphologies. We point out that there exists an out-of-plane stress component within full pyramids due to their 3D geometry, which can act as a driving force for the motion of the misfit dislocation on the basal plane from their edges toward their center. This out-of-plane stress component is due to the fact that the misfit dislocation cannot completely relieve the lattice-mismatch-induced strain when located at the edges of full pyramids. The misfit dislocation thus moves from the edges of full pyramids toward their center so as to favor complete strain relaxation, as depicted by the schematic in Fig. 7: once the misfit dislocation reaches the center, a shape transition toward the NW morphology takes place.
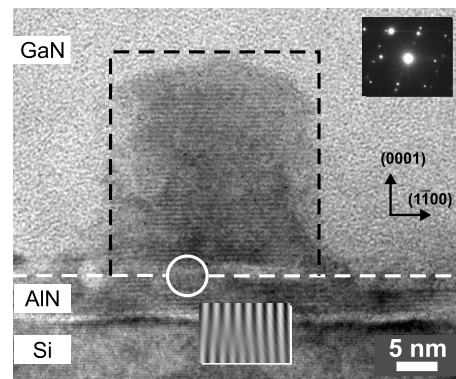

FIG. 6. HRTEM image of a dislocated NW collected on a sample grown during 15 min. The misfit dislocation is located within the white circle, which is close to the center of the NW. The inset reveals a Fourier-filtered enhancement showing only the $\{1\bar{1}00\}$ lattice planes. The dislocation is again mixed with a Burgers vector of $(1/3)\langle 11\bar{2}0\rangle$ and retains a dominant edge component. A SAED pattern of the dislocated NW also reveals that the NW is completely relaxed.
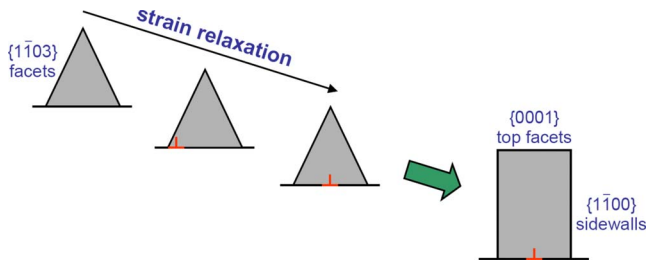
FIG. 7. (Color online) Schematic of the physical mechanisms at work during the final shape transition from full pyramids toward the very first NWs. The cross icon represents the misfit dislocation, which moves from the edges toward the center of full pyramids in order to ensure a complete relaxation of the lattice-mismatch-induced strain.

As a consequence, our experimental observations suggest that the nucleation of at least one misfit dislocation is essential for the self-induced formation of epitaxial GaN NWs, although it occurs within full pyramids. Such a nucleation of the misfit dislocation favors the subsequent shape transition from dislocated full pyramids to dislocated NWs by entirely relieving the lattice-mismatch-induced strain. In the following, we discuss the role of plastic relaxation process on the driving force for this final shape transition through thermodynamic considerations. We also draw some direct relationships between these thermodynamics aspects and the specific conditions used for the self-induced growth of GaN NWs.

IV. DISCUSSION

Several theoretical approaches are based on thermodynamics considerations to account for the shape transitions occurring during the QD growth, in the silicon/germanium material system, for instance.[35,38,39,51] These approaches mainly state that the preferential island shape is given by the minimization of its total free energy per unit volume. In other words, the strong variation in the total free energy for two distinct morphologies can induce a significant driving force resulting in a shape transition: it is expected that, for a given volume, the total free energy is significantly smaller for dislocated NWs than for dislocated full pyramids. Several types of distinct energies contribute to such a driving force:[51,52] the shape transitions are mainly driven by the interplay between the stored elastic strain energy and the total interface and surface energy of all the facets composing the dislocated full pyramids and the dislocated NWs, respectively. The elastic strain energy can originate from the strain induced by the lattice mismatch and the strain induced by surface stress, which is here neglected due to the large size of full pyramids. Yet, once the misfit dislocation reaches the center of full pyramids, the lattice-mismatch-induced strain is completely relieved so that only the edge contribution may be involved in the elastic strain energy. A local strain related to the discontinuity of the intrinsic surface stress tensor at island edges can be important, as discussed by Shchukin *et al.*[52] Nevertheless, the ratio of the typical dimensions of edges over the radius of full pyramids is relatively low so that edge effects could only play a minor role in the driving force of the final shape transition. A similar argument can also be mentioned concerning the edge energy. In addition, given that the final shape transition occurs between dislocated full pyramids and dislocated NWs with similar radii, the interface area does not change significantly between the two different morphologies: this statement indicates that the increase in the interface area costs a very large energy, which prevents in turn the interface from spreading itself. One can thus exclude that the interface energy contributes to the driving force of the final shape transition since the interface area remains constant for both dislocated full pyramids and dislocated NWs.

Consequently, only the surface energy can play a major role in such a shape transition: indeed, full pyramids and NWs present different types of facets. Yet, the value of the surface energy depends on the crystallographic orientation of the involved facets.[53] It is well established that the close-packed planes, namely, the {0001} planes in the wurtzite structure, generally retain a very low surface energy. The surface energies of {0001} and {1$\bar{1}$00} planes are thus relatively small with respect to the surface energy of {1$\bar{1}$03} facets, which is expected to be higher.[53,54] Nevertheless, no value for the surface energy of {1$\bar{1}$03} facets is mentioned in the literature. One can however maintain that, once the lattice-mismatch-induced strain vanishes, the driving force for the final shape transition is governed by the anisotropy of surface energy and by edge effects, as the respective major and minor contributions. Simple thermodynamic considerations can therefore account for the preferential growth of NWs starting from dislocated full pyramids, which are completely relaxed.

Some growth considerations in the MBE chamber could also favor the final shape transition since gallium and nitrogen atoms are supplied in such a way that it may easily arrange into a new island shape, in correlation with geometric effects, for instance.[27] Varying the growth temperature or the V/III ratio can directly change the time scale and even the nature of the physical mechanisms involved; this can also be the case when increasing the lattice mismatch: such a growth could induce a shorter time scale for all the nucleation process described here, limiting, for instance, the nature and the number of the shapes involved. It could also result in a plastic relaxation process involving a larger number of misfit dislocations and occurring at smaller critical sizes. However, it is expected that the nucleation processes for the self-induced growth of epitaxial GaN NWs on highly lattice-mismatched substrates is similar as regards the general aspects discussed here. In other words, the specific growth conditions for GaN NWs play a critical role. A high V/III ratio is required and often combined with a high growth temperature.[13–16] As the surface energy of a given plane highly depends on its orientation and on the surface reconstruction at work, the control of the V/III ratio is crucial.[55] Indeed, the anisotropy of surface energy as the main driving force could be efficient enough to favor the NW formation and growth in an appropriate range of V/III ratio: in other words, the modulation of surface energy for {0001}, {1$\bar{1}$00}, and {1$\bar{1}$03} facets may induce the final shape transition toward the NW morphology only if highly nitrogen-rich conditions are strictly used.

V. CONCLUSION

We have investigated the nucleation mechanisms during the self-induced growth of epitaxial GaN NWs by combining *in situ* RHEED measurements and *ex situ* HRTEM imaging: it is found that GaN nucleates coherently strained on the AlN buffer layer as spherical-cap-shaped islands before a complete continuous 2D wetting layer has been formed. No sign for the presence of a GaN wetting layer is observed from HRTEM images. Several consecutive shape transitions from spherical caps through truncated- to full-pyramid-shaped islands have been observed and identified at the onset of the nucleation process: such islands can thus reduce their total free energy per unit volume by elastically relieving the lattice-mismatch-induced strain with the newly formed facets. Beyond critical sizes, the plastic relaxation process occurs through the nucleation of one misfit dislocation at the island edges of full pyramids. The experimental critical radius is in very good agreement with the theoretical critical radius for the formation of one misfit dislocation in full pyramids, as given by the approach of Tillmann and Förster,[28] but smaller than the theoretical critical radius predicted in cylindrical-shaped NWs, as given by the approach of Glas.[29] Once the misfit dislocation reaches the spatial position where it most efficiently relieves the lattice-mismatch-induced strain within full pyramids, namely, close to their center, the final shape transition to the very first GaN NWs takes place. We have associated such a shape transition from dislocated full pyramids toward dislocated NWs with the complete relaxation of the lattice-mismatch-induced strain related to the plastic relaxation process: this strain relaxation results in a significant difference in the total free energy per unit volume for both types of morphologies. In particular, we have argued that the driving force for such a shape transition is in the majority driven by the anisotropy of surface energy, even if edge effects could also play a role. Furthermore, we have emphasized the importance of a high V/III ratio, as it has in the self-induced growth of GaN NWs a direct influence on the value of the surface energy for all the facets involved in the different island shapes.

These findings reveal that such self-induced GaN NWs epitaxially grown on the AlN buffer layer do contain at least one misfit dislocation, which is necessary for their own formation. Furthermore, these findings also show that the initial radius of the very first GaN NWs corresponds to the critical radius required to nucleate the misfit dislocation within full pyramids. As a consequence, varying the initial radius of self-induced epitaxial GaN NWs requires to adapt the material system, namely, the value of the lattice mismatch, by changing either the substrate or the buffer layer.

[1] C. M. Lieber and Z. L. Wang, MRS Bull. **32**, 99 (2007).

[2] M. H. Huang, S. Mao, H. Feick, H. Yan, Y. Wu, H. Kind, E. Weber, R. Russo, and P. Yang, Science **292**, 1897 (2001).

[3] Y. Cui, Q. Wei, H. Park, and C. M. Lieber, Science **293**, 1289 (2001).

[4] M. T. Bjork, B. J. Ohlsson, T. Sass, A. I. Persson, C. Thelander, M. H. Magnusson, K. Deppert, L. R. Wallenberg, and L. Samuelson, Appl. Phys. Lett. **80**, 1058 (2002).

[5] M. Law, L. E. Greene, J. C. Johnson, R. Saykally, and P. Yang, Nature Mater. **4**, 455 (2005).

[6] R. S. Wagner and W. C. Ellis, Appl. Phys. Lett. **4**, 89 (1964).

[7] V. G. Dubrovskii, N. V. Sibirev, J. C. Harmand, and F. Glas, Phys. Rev. B **78**, 235301 (2008).

[8] B. A. Wacaser, K. A. Dick, J. Johansson, M. T. Borgström, K. Deppert, and L. Samuelson, Adv. Mater. (Weinheim, Ger.) **21**, 153 (2009).

[9] M. C. Putnam, M. A. Filler, B. M. Kayes, M. D. Kelzenberg, Y. Guan, N. S. Lewis, J. M. Eiler, and H. A. Atwater, Nano Lett. **8**, 3109 (2008).

[10] S. H. Oh, K. van Benthem, S. I. Molina, A. Y. Borisevich, W. Luo, P. Werner, N. D. Zakharov, D. Kumar, S. T. Pantelides, and S. J. Pennycook, Nano Lett. **8**, 1016 (2008).

[11] D. E. Perea, J. E. Allen, S. J. May, B. W. Wessels, D. N. Seidman, and L. J. Lauhon, Nano Lett. **6**, 181 (2006).

[12] N. Wang, Y. Cai, and R. Q. Zhang, Mater. Sci. Eng. R. **60**, 1 (2008).

[13] M. Yoshizawa, A. Kikuchi, M. Mori, N. Fujita, and K. Kishino, Jpn. J. Appl. Phys., Part 2 **36**, L459 (1997).

[14] M. A. Sanchez-Garcia, E. Calleja, E. Monroy, F. J. Sanchez, F. Calle, E. Muñoz, and R. Beresford, J. Cryst. Growth **183**, 23 (1998).

[15] K. A. Bertness, A. Roshko, N. A. Sanford, J. M. Barker, and A. V. Davydov, J. Cryst. Growth **287**, 522 (2006).

[16] R. Meijers, T. Richter, R. Calarco, T. Stoica, H.-P. Bochem, M. Marso, and H. Lüth, J. Cryst. Growth **289**, 381 (2006).

[17] R. Songmuang, O. Landré, and B. Daudin, Appl. Phys. Lett. **91**, 251902 (2007).

[18] R. Calarco, R. Meijers, R. K. Debnath, T. Stoica, E. Sutter, and H. Lüth, Nano Lett. **7**, 2248 (2007).

[19] K. A. Bertness, A. Roshko, L. M. Mansfield, T. E. Harvey, and N. A. Sanford, J. Cryst. Growth **300**, 94 (2007).

[20] T. Stoica, E. Sutter, R. J. Meijers, R. K. Debnath, R. Calarco, H. Lüth, and D. Grützmacher, Small **4**, 751 (2008).

[21] H. W. Seo, Q. Y. Chen, L. W. Tu, C. L. Hsiao, M. N. Iliev, and W. K. Chu, Phys. Rev. B **71**, 235314 (2005).

[22] S. Guha, N. Bojarczuk, M. Jonhson, and J. Schetzina, Appl. Phys. Lett. **75**, 463 (1999).

[23] E. Calleja, M. A. Sánchez-García, F. J. Sánchez, F. Calle, F. B. Naranjo, E. Muñoz, U. Jahn, and K. Ploog, Phys. Rev. B **62**, 16826 (2000).

[24] J. Ristíc, E. Calleja, S. Fernández-Garrido, L. Cerutti, A. Trampert, U. Jahn, and K. H. Ploog, J. Cryst. Growth **310**, 4035 (2008).

[25] K. A. Bertness, A. Roshko, L. M. Mansfield, T. E. Harvey, and

N. A. Sanford, J. Cryst. Growth **310**, 3154 (2008).

[26] L. Lymperakis and J. Neugebauer, Phys. Rev. B **79**, 241308(R) (2009).

[27] C. T. Foxon, S. V. Novikov, J. L. Hall, R. P. Campion, D. Cherns, I. Griffiths, and S. Khongphetsak, J. Cryst. Growth **311**, 3423 (2009).

[28] K. Tillmann and A. Förster, Thin Solid Films **368**, 93 (2000).

[29] F. Glas, Phys. Rev. B **74**, 121302(R) (2006).

[30] K. Shimada, T. Sota, and K. Suzuki, J. Appl. Phys. **84**, 4951 (1998).

[31] C. Ratsch and J. A. Venables, J. Vac. Sci. Technol. A **21**, S96 (2003).

[32] B. Daudin, F. Widmann, G. Feuillet, Y. Samson, M. Arlery, and J. L. Rouvière, Phys. Rev. B **56**, R7069 (1997).

[33] N. Gogneau, D. Jalabert, E. Monroy, T. Shibata, M. Tanaka, and B. Daudin, J. Appl. Phys. **94**, 2254 (2003).

[34] D. J. Eaglesham and M. Cerullo, Phys. Rev. Lett. **64**, 1943 (1990).

[35] J. Tersoff and F. K. LeGoues, Phys. Rev. Lett. **72**, 3570 (1994).

[36] M. Arlery, J. L. Rouvière, F. Widmann, B. Daudin, G. Feuillet, and H. Mariette, Appl. Phys. Lett. **74**, 3287 (1999).

[37] M. Korytov, M. Benaissa, J. Brault, T. Huault, T. Neisius, and P. Vennéguès, Appl. Phys. Lett. **94**, 143105 (2009).

[38] I. Daruka, J. Tersoff, and A. L. Barabási, Phys. Rev. Lett. **82**, 2753 (1999).

[39] J. Tersoff, B. J. Spencer, A. Rastelli, and H. von Känel, Phys. Rev. Lett. **89**, 196104 (2002).

[40] M. Knelangen, V. Consonni, A. Trampert, and H. Riechert (unpublished).

[41] M. Krishnamurthy, J. S. Drucker, and J. A. Venables, J. Appl. Phys. **69**, 6461 (1991).

[42] J. Drucker, Phys. Rev. B **48**, 18203 (1993).

[43] J. W. Matthews and A. E. Blakeslee, J. Cryst. Growth **27**, 118 (1974).

[44] H. T. Johnson and L. B. Freund, J. Appl. Phys. **81**, 6081 (1997).

[45] A. F. Wright, J. Appl. Phys. **82**, 2833 (1997).

[46] R. B. Schwarz, K. Khachaturian, and E. R. Weber, Appl. Phys. Lett. **70**, 1122 (1997).

[47] G. E. Cirlin, V. G. Dubrovskii, I. P. Soshnikov, N. V. Sibirev, Yu. B. Samsonenko, A. D. Bouravleuv, J. C. Harmand, and F. Glas, Phys. Status Solidi (RRL) **3**, 112 (2009).

[48] S. Guha, A. Madhukar, and K. C. Rajkumar, Appl. Phys. Lett. **57**, 2110 (1990).

[49] B. J. Spencer and J. Tersoff, Phys. Rev. B **63**, 205424 (2001).

[50] A. Marzegalli, V. A. Zinovyev, F. Montalenti, A. Rastelli, M. Stoffel, T. Merdzhanova, O. G. Schmidt, and L. Miglio, Phys. Rev. Lett. **99**, 235505 (2007).

[51] V. A. Shchukin, N. N. Ledentsov, P. S. Kop'ev, and D. Bimberg, Phys. Rev. Lett. **75**, 2968 (1995).

[52] V. A. Shchukin and D. Bimberg, Rev. Mod. Phys. **71**, 1125 (1999).

[53] J. E. Northrup and J. Neugebauer, Phys. Rev. B **53**, R10477 (1996).

[54] J. E. Northrup, J. Neugebauer, R. M. Feenstra, and A. R. Smith, Phys. Rev. B **61**, 9932 (2000).

[55] A. R. Smith, R. M. Feenstra, D. W. Greve, J. Neugebauer, and J. E. Northrup, Phys. Rev. Lett. **79**, 3934 (1997).